Ab initio study of thermodynamic, electronic, magnetic, structural, and elastic properties of Ni_4N allotropes

P. Hemzalová,[1,2,3] M. Friák,[2,3,4,*] M. Šob,[3,4,1] D. Ma,[2] A. Udyansky,[2] D. Raabe,[2] and J. Neugebauer[2]

[1]*Department of Chemistry, Faculty of Science, Masaryk University, Kotlářská 2, CZ-611 37 Brno, Czech Republic*

[2]*Max-Planck-Institut für Eisenforschung GmbH, Max-Planck-Str. 1, D-40237 Düsseldorf, Germany*

[3]*Central European Institute of Technology, CEITEC MU, Masaryk University, Kamenice 5, CZ-625 00 Brno, Czech Republic*

[4]*Institute of Physics of Materials, Academy of Sciences of the Czech Republic, v.v.i., Žižkova 22, CZ-616 62 Brno, Czech Republic*

(Received 21 December 2012; revised manuscript received 30 September 2013; published 12 November 2013)

We have employed parameter-free density functional theory calculations to study the thermodynamic stability and structural parameters as well as elastic and electronic properties of Ni_4N in eight selected crystallographic phases. In agreement with the experimental findings, the cubic structure with Pearson symbol cP5, space group $Pm\bar{3}m$ (221) is found to be the most stable and it is also the only thermodynamically stable structure at $T = 0$ K with respect to decomposition to the elemental Ni crystal and N_2 gas phase. We determine structural parameters, bulk moduli, and their pressure derivatives for all eight allotropes. The thermodynamic stability and bulk modulus is shown to be anticorrelated. Comparing ferromagnetic and nonmagnetic states, we find common features between the magnetism of elemental Ni and studied ferromagnetic Ni_4N structures. For the ground-state Ni_4N structure and other two Ni_4N cubic allotropes, we predict a complete set of single-crystalline elastic constants (in the equilibrium and under hydrostatic pressure), the Young and area moduli, as well as homogenized polycrystalline elastic moduli obtained by different homogenization methods. We demonstrate that the elastic anisotropy of the ground-state Ni_4N is qualitatively opposite to that in the elemental Ni, i.e., these materials have hard and soft crystallographic directions interchanged. Moreover, one of the studied metastable cubic phases is found auxetic, i.e., exhibiting negative Poisson ratio.

DOI: 10.1103/PhysRevB.88.174103 PACS number(s): 62.20.de, 71.20.Be, 75.50.Cc

I. INTRODUCTION

Nickel nitrides are binary compounds of great importance for numerous industrial applications, e.g., when manufacturing electronic devices with GaN contacts[1–4] or producing Ni-containing stainless steels (see, e.g., Refs. 5 and 6). As far as the production of electronics is concerned, nickel nitrides appear in nickel thin films when manufacturing electronic chips and may have major influence on their conductivity. During the fabrication, nickel metal is first evaporated and afterwards deposited onto the basal surface, and the apparatus is irrigated by inert nitrogen atmosphere. As a result, nitrides may substantially alter technological properties of surface layers.

In the steel production, surfaces can be nitrided in order to increase their hardness via forming a variety of nitrides (see, e.g., Refs. 7–10). They improve, e.g., the strength of austenitic steels by forming nitrides at grain boundaries due to the very low solubility of nitrides. Motivated by these industrial applications, properties of nickel nitrides have been studied employing various experimental methods, including ordering tendencies of N atoms by neutron diffraction[11] or (100) surface reconstructions by scanning tunneling microscopy.[12]

A direct synthesis of nickel nitrides from nickel and nitrogen in laboratory conditions has not yet been reported. The value of the equilibrium pressure can be only estimated and is assumed to be very high.[11] Chemically pure nickel nitrides can be prepared at high temperatures, e.g., by the reduction of ammonia and nickel monoxide. The first reported synthesis of hexagonal Ni_3N was performed at 450 °C and nickel powder and liquid ammonia were used.[11] When applying the disproportionation on Ni_3N at 650 K, two other nickel nitrides can be synthesized,[13] namely cubic Ni_4N and face-centered Ni_8N (with the elementary unit cell $Ni_{32}N_4$).

Alternatively, when employing the thermal decomposition of metal precursors in a supercritical ammonia-methanol mixture, nanostructured nitrides can be produced.[14] Using nickel amidinate precursor and either ammonia (NH_3) or a mixture of NH_3 and hydrogen (H_2) gases as coreactants, smooth and continuous films of Ni_xN (with the Ni/N atomic ratio ranging from 3:1 to 15:1) with excellent step coverage were deposited.[15]

As another synthesis route, nickel nitrides can be produced by sputtering of a nickel target with a beam of nitrogen ions that results in the formation of crystalline nickel nitride, which is deposited on cold surfaces surrounding the target.[16] When adding also Ti atoms, titanium-nickel nitride coatings (Ti-Ni-N) by unbalanced magnetron sputtering with a pulsed dc discharge at the targets may be produced.[17] Similarly, nickel layers can be implanted with nitrogen using plasma-based ion implantation in order to form Ni nitrides.[18] Using state-of-the-art preparation techniques, nitrides of other metals (such as Fe_4N or Co_4N) were prepared[19] including even the first binary nitride of the noble metals group (PtN) that was recently synthesized.[20]

Despite the experimental studies partly summarized above, relatively very little is known about materials characteristics of these nitrides. Therefore, we employ quantum-mechanical calculations in order to shed more light on thermodynamic, electronic, structural, magnetic, and elastic properties of this important class of materials. In the present study we focus on Ni_4N. This compound is considered metastable based on previous thermodynamic assessments of Ni-N system.[21–23] When synthesized, Ni_4N was experimentally found[13,24–26] to crystallize in a simple cubic structure with a five-atom basis (Pearson's symbol cP5, space group $Pm\bar{3}m$ (221), prototype Fe_4N or CaO_3Ti). The nitrogen atom is situated at the position

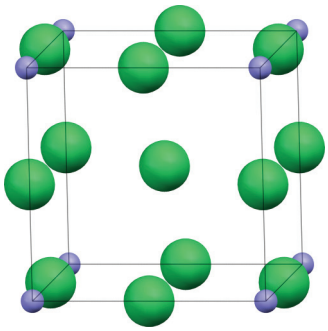

FIG. 1. (Color online) Schematic figure of the experimentally observed ground state of Ni_4N cubic allotrope (referred to as α-Ni_4N in the text below). The Ni atoms are shown as larger green and the N ones as smaller blue spheres.

1a (0, 0, 0) and the Ni atoms at the positions 1b (1/2, 1/2, 1/2), and 3d (1/2, 0, 0), (0, 1/2, 0) a (0, 0, 1/2); see Fig. 1. Alternative to this crystallographic phase, Ni_4N in another cubic phase as well as in a tetragonal allotrope has been described in Refs. 27 and 28.

In this paper we extend our previous study of nickel nitrides,[29] where the focus was on the experimental cubic Ni_4N ground-state phase, to seven metastable structural phases with the same stoichiometry. We examine the thermodynamic stability of various Ni_4N allotropes (Tables I and II), determine their structural parameters, and compare them with the results of previous theoretical and experimental studies. Subsequently we predict both single-crystalline elastic constants and homogenized polycrystalline moduli of three cubic Ni_4N allotropes (the ground-state phase Ni_4N and of two other cubic phases) and their electronic structure characteristics.

The paper is organized as follows. After Introduction, the Methodology section describes our computational method, provides computational parameters, summarizes crystallographic characteristics of all studied allotropes, and introduces our approach to the determination of both single-crystalline and polycrystalline elastic properties. In Sec. III we first compare thermodynamic, structural, and elastic properties of studied allotropes and analyze relations between thermodynamic stability and the bulk modulus. Subsequently we focus on calculated properties of the Ni_4N in the ground state. After studying its magnetic properties (also in comparison with fcc Ni), we further provide its electronic-structure characteristics and then analyze elastic properties at both zero pressure as well as at hydrostatic pressures ranging from tensile to compressive loads. The elastic characteristics, including Poisson ratios, of the ground-state phase are then compared to two other studied cubic phases. Section IV then summarizes the results and concludes the paper.

TABLE I. Crystallographic description of the six studied Ni_4N allotropes (labeled by Greek symbols from α to θ) including space groups and their corresponding numbers as well as Wyckoff positions and prototype compounds. Also added is the number of **k** points used for each compound in our *ab initio* calculations. Two other allotropes studied, i.e., Lifshitz structures β-Ni_4N and δ-Ni_4N, are visualized below in Figs. 3 and 2 and described separately in Table II (before the structural optimization). The optimized atomic positions in the β-Ni_4N and δ-Ni_4N phases are given in Tables X and XI (see the Appendix).

Ni_4N	α	γ	ε	ζ	η	θ
Group	$Pm\bar{3}m$	$Pnma$	$Pmmm$	$P43m$	$I43m$	$P4/nmm$
Group no.	221	62	47	215	217	129
Pearson	cP5	oP20	oP5	cP5	cI10	tP10
Positions N	1a	4c	1h	1a	2a	2c
Positions Ni	1b, 3d	4c, 8d	1a, 1b, 2l	4e	8c	2a, 2c, 4f
No. of u	0	7	1	1	1	3
Prototype	Fe_4N	B_4Mg	Ta_4O	Fe_4C	F_4Si	Be_4B
k points	40 000	38 400	40 320	40 000	40 960	38 880

TABLE II. Unrelaxed atomic positions (before full structural optimization) in the two cubic Lifshitz structures β-Ni_4N and δ-Ni_4N that differ in Wyckoff positions of N atoms but have equal Wyckoff positions of Ni atoms. Internal atomic positions that are not dictated by symmetry are defined by internal parameters. For these we use the following general form ${}^{A}u^{B\text{-}C}$ where A specifies atom (Ni or N), B is for the direction x, y or z, and C is the name of a given Wyckoff sublattice. If B is not specified, the internal parameter is valid for both Ni and N atoms. If C is not used, the Wyckoff sublattice does not have a standardized name. Relaxed values of internal parameter of β-Ni_4N and also of other allotropes are listed in Table XI. The exact atomic positions of Ni atoms (after full structural optimization) in δ-Ni_4N allotrope are listed in Table X.

β-Ni_4N	δ-Ni_4N
Nitrogen Wyckoff positions	
(1/4, 1/4, 1/4)	(0, 0, 0)
(3/4, 3/4, 1/4)	(1/2, 1/2, 1/2)
(3/4, 1/4, 3/4)	(1/4, 3/4, 1/4)
(1/4, 3/4, 3/4)	(3/4, 1/4, 3/4)
Nickel Wyckoff positions (same in β-Ni_4N and δ-Ni_4N)	
(1/4, 0, 0); (1/4, 1/2, 0)	
(3/4, 0, 0); (3/4, 1/2, 0)	
(1-${}^{Ni}u^{x}$, 1/4, 1/4); (${}^{Ni}u^{x}$, 3/4, 1/4)	
(1/2+${}^{Ni}u^{x}$, 1/4, 1/4); (1/2-${}^{Ni}u^{x}$, 3/4, 1/4)	
(1/4, 0, 1/2); (1/4, 1/2, 1/2)	
(3/4, 0, 1/2); (3/4, 1/2, 1/2)	
(${}^{Ni}u^{x}$, 1/4, 3/4); (1-${}^{Ni}u^{x}$, 3/4, 3/4)	
(1/2-${}^{Ni}u^{x}$, 1/4, 3/4); (1/2+${}^{Ni}u^{x}$, 3/4, 3/4)	

II. METHODOLOGY

A. Computational details

Our *ab initio* calculations are based on density functional theory (DFT)[30,31] using the generalized gradient approximation (GGA)[32] and the projector augmented wave approach (PAW) as implemented in the VASP code.[33–35] The plane-wave cutoff energy is 360 eV and the Monkhorst-Pack[36] scheme is used to sample the Brillouin zone. Convergence with respect to cutoff energy and **k**-point sampling has been explicitly checked (for details, see Table I). In all cases studied, we started our calculations with the Ni atoms ferromagnetically spin polarized and we allowed for a full structural relaxation, i.e., the total energy was minimized as a function of both internal atomic positions, the unit-cell shape as well as the volume. We chose the Methfessel-Paxton scheme[37] for the Fermi level smearing and the corresponding smearing parameter equals to 0.1 eV.

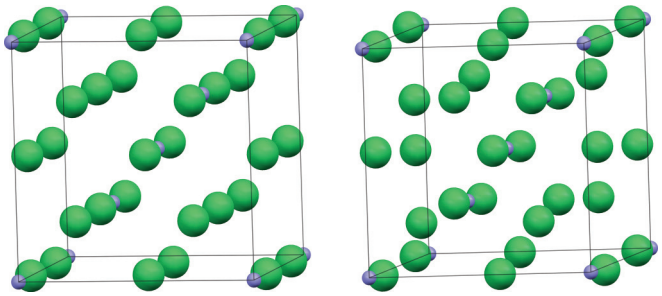

FIG. 2. (Color online) Schematic visualization of the Lifshitz structural allotrope δ-Ni_4N before structural relaxation (left) and after full geometry optimization of both the cell shape and internal atomic positions (right) with the Ni atoms shown as larger green and the N ones as smaller blue spheres.

B. Description of crystal structures

The *ab initio* calculations have been performed for a series of different crystallographic variants that are labeled according to their formation energy (see a detailed discussion below) with respect to the experimentally observed ground-state phase using the Greek alphabet (the ground-state phase is then denoted as α-Ni_4N). Our choice of the structures (see Tables I and II) was motivated by experimental findings of another unidentified cubic Ni_4N phase and one tetragonal Ni_4N allotrope. We thus propose a few possible candidates and hope that our theoretical study will trigger an experimental investigation of these yet unidentified phases.

C. *Ab initio* calculations of elastic constants

Single-crystal elastic constants C_{ij} can be routinely obtained from *ab initio* calculated changes of the total energy as a function of specific lattice distortions applied to the undistorted ground state (see, e.g., Refs. 38 and 39). For a cubic crystal (such as cP5 or cI10 phases of Ni_4N) three elastic constants are needed, i.e., three different distortions have to be simulated. The first one is the isotropic volume change providing the energy-volume dependence, where the second derivative at the minimum of the energy-volume curve determines the bulk modulus B. Here we employ the Murnaghan equation of state.[40] The bulk modulus can also be expressed as a linear combination of two elastic constants:

$$V\left(\frac{\partial^2 E}{\partial V^2}\right)_{V_{\mathrm{eq}}} = \frac{1}{3}(C_{11} + 2C_{12}) = B. \qquad (1)$$

As the phase with the alternative cubic structure has not been clearly described in literature, we have analyzed a few frequently occurring binary structures with the 4:1 stoichiometry as well as two Lifshitz structures (see, e.g., Refs. 41–43) β-Ni_4N and δ-Ni_4N as structural models of interstitial solid solutions of N in Ni. In Tables I and II (and also in Tables X and XI in the Appendix) we summarize crystallographic characteristics of all studied allotropes that are also depicted in Figs. 1–5. Atomic positions in Lifshitz structures β-Ni_4N and δ-Ni_4N prior structural optimization are summarized in Table II. As the structure optimization resulted in rather significant changes in these atomic positions in the case of δ-Ni_4N, the structure-optimized (relaxed) atomic positions are given in Table X in the Appendix.

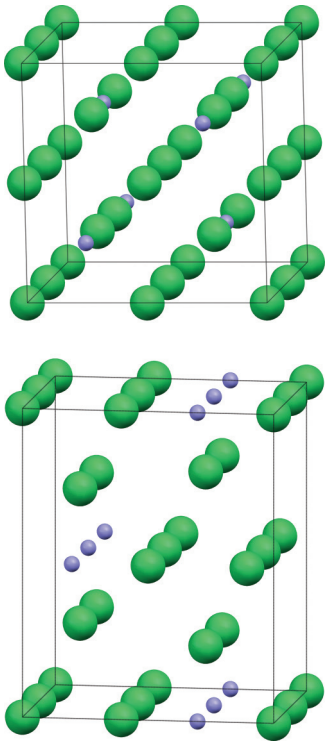

FIG. 3. (Color online) Lifshitz structural allotrope β-Ni_4N (upper panel) and the γ-Ni_4N phase (lower panel). The Ni atoms are shown as larger green and the N ones as smaller blue spheres.

The other two deformations were chosen as uniaxial distortions along the [001] and [111] directions and these can be expressed by the following strain matrices:

$$\epsilon^{[001]} = \begin{pmatrix} \delta/2 & 0 & 0 \\ 0 & \delta/2 & 0 \\ 0 & 0 & \frac{1}{(1+\delta/2)^2} - 1 \end{pmatrix}, \qquad (2)$$

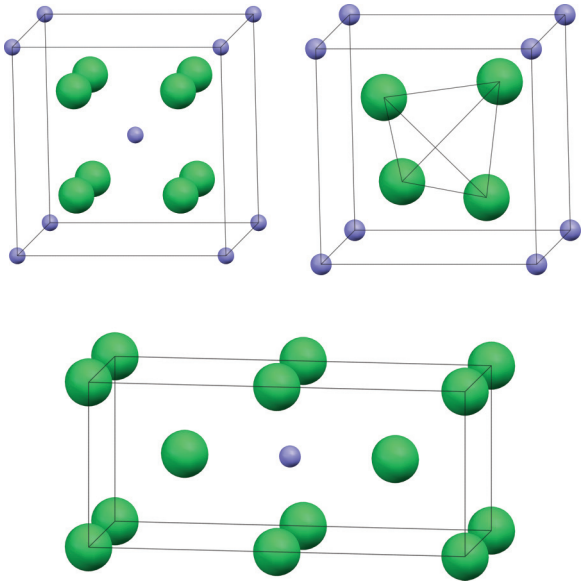

FIG. 4. (Color online) Structural allotropes η-Ni_4N (upper left), ζ-Ni_4N (upper right), and ε-Ni_4N (lower panel) with the Ni atoms shown as larger green and the N ones as smaller blue spheres.

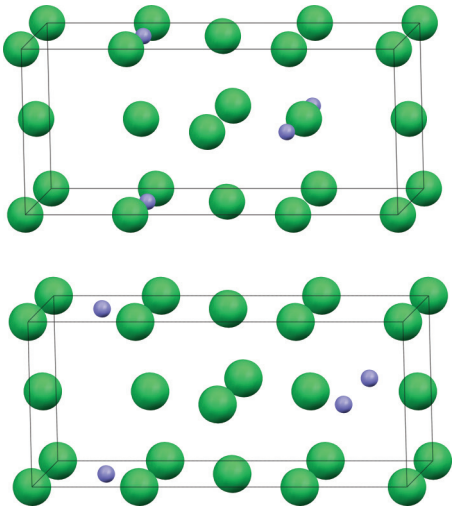

FIG. 5. (Color online) Visualization of structural allotrope θ-Ni_4N before structural relaxation (upper panel) and after full geometry optimization of both the cell shape and internal atomic positions (lower panel) with the Ni atoms shown as larger green and the N ones as smaller blue spheres.

$$\epsilon^{[111]} = \begin{pmatrix} 0 & \delta/2 & \delta/2 \\ \delta/2 & 0 & \delta/2 \\ \delta/2 & \delta/2 & 0 \end{pmatrix}, \tag{3}$$

where δ is a parameter characterizing the magnitude of strain. In this study, the maximum lattice distortion was limited to ± 0.04 in order to avoid nonlinearities. The corresponding changes of the total energy $E(\delta)$ with respect to the energy of the ground state E_0 are then divided by the volume V in order to calculate the elastic energy density $U(\delta)$. This density is linked for each kind of distortion to specific elastic constants as

$$\frac{\partial^2 U^{[001]}}{\partial \delta^2} = \frac{3}{2}(C_{11} - C_{12}) = 3C', \tag{4}$$

$$\frac{\partial^2 U^{[111]}}{\partial \delta^2} = 3C_{44}. \tag{5}$$

Since in essentially all synthesis routes polycrystalline rather than single-crystalline material is produced, single-crystal elastic constants are homogenized in a scale-bridging manner. To predict elastic moduli, such as the shear modulus G or Young modulus Y, various homogenization approaches have been proposed in the past. The Voigt scheme[44] assumes that the local strain is equal in all the grains of a polycrystal and the corresponding polycrystalline shear modulus G_V is then expressed as

$$G_V = \frac{C_{11} - C_{12} + 3C_{44}}{5} = \frac{2C' + 3C_{44}}{5}. \tag{6}$$

The Reuss homogenization[45] is based on the assumption of a constant local stress and the corresponding polycrystalline shear modulus G_R can be expressed as a function of elastic compliances S_{ij}:

$$G_R = \frac{5}{4(S_{11} - S_{12}) + 3S_{44}}. \tag{7}$$

Here the relationship between S_{ij} and C_{ij} for materials with cubic symmetry is

$$S_{11} = \frac{C_{11} + C_{12}}{(C_{11} - C_{12})(C_{11} + 2C_{12})}, \tag{8}$$

$$S_{12} = \frac{-C_{12}}{(C_{11} - C_{12})(C_{11} + 2C_{12})}, \tag{9}$$

$$S_{44} = \frac{1}{C_{44}}. \tag{10}$$

Equation (7) can be rewritten in terms of C_{ij} as

$$G_R = \frac{5(C_{11} - C_{12})C_{44}}{4C_{44} + 3(C_{11} - C_{12})} = \frac{10C'C_{44}}{4C_{44} + 6C'}. \tag{11}$$

For the Hershey method, the homogenized polycrystalline shear modulus G_H is given as a root of a polynomial. Two different expressions of this polynomial are available in the literature. The original paper by Hershey[46] gives the following quartic equation:

$$\begin{aligned} &64G_H^4 + 16(4C_{11} + 5C_{12})G_H^3 + [3(C_{11} + 2C_{12}) \\ &\times (5C_{11} + 4C_{12}) - 8(7C_{11} - 4C_{12})C_{44}]G_H^2 \\ &- (29C_{11} - 20C_{12})(C_{11} + 2C_{12})C_{44}G_H \\ &- 3(C_{11} + 2C_{12})^2(C_{11} - C_{12})C_{44} = 0. \end{aligned} \tag{12}$$

This fourth-order polynomial is used in the majority of recently published papers (see, e.g., Refs. 38, 47, and 48), but it can be transformed to a third-order polynomial (Refs. 49–51),

$$\begin{aligned} &G_H^3 + \tfrac{1}{8}(5C_{11} + 4C_{12})G_H^2 - \tfrac{1}{8}C_{44}(7C_{11} - 4C_{12})G_H \\ &- \tfrac{1}{8}C_{44}(C_{11} - C_{12})(C_{11} + 2C_{12}) = 0, \end{aligned} \tag{13}$$

proposed by Ledbetter.[52] For systems fulfilling the conditions of mechanical stability, i.e., $B > 0$, $C_{44} > 0$, $C' > 0$, both Eqs. (12) and (13) change the sign of their coefficients only once and therefore have only one real root for a given set of elastic constants. This single root is identical in Eqs. (12) and (13).

Another computationally very simple method has been proposed by Hill[53] and Gilvarry.[54] This is the Reuss-Voigt-Hill-Gilvarry (RVHG) method according to which the polycrystalline shear modulus is assumed to be the arithmetic mean of the Reuss and Voigt values:

$$G_{RVHG} = \tfrac{1}{2}(G_R + G_V). \tag{14}$$

The homogenized bulk modulus B_0 for systems with cubic symmetry as considered here is given by the same expression, Eq. (1), in all four methods.

Once the homogenized elastic constants are known, other homogenized elastic quantities, such as the Young modulus Y or Poisson ratio ν, can be easily obtained:

$$Y = \frac{9B_0G}{3B_0 + G}, \quad \nu = \frac{1}{2}\frac{3B_0 - 2G}{3B_0 + 2G}. \tag{15}$$

Here, G is equal to G_V, G_R, G_H, or G_{RVHG}.

III. RESULTS AND DISCUSSION

The computed dependences of the differences in the total energy ΔE_{TOT} (in eV per atom) as a function of volume V for different structural variants are displayed in Fig. 6. The phase with the lowest value of the total energy in its equilibrium

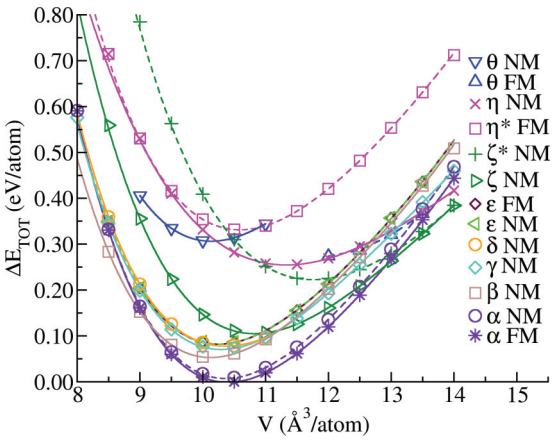

FIG. 6. (Color online) Total energy with respect to the minimum of the ground-state energy ΔE_{TOT} as a function of volume V (in Å^3 per atom) for different ferromagnetic (FM) and nonmagnetic (NM) Ni_4N allotropes. Curves η^* and ζ^* correspond to states with the internal parameters kept constant and equal to 0.25 (see the explanation in Sec. III).

state, and therefore the most stable structure, is the α-Ni_4N allotrope in agreement with experimental findings; all total energy differences are computed with respect to this energy. Let us note that in case of the θ-Ni_4N, we have encountered convergence problems in the region of volumes of 11-12 Å^3 where we detected a phase transition from the FM state (at higher volumes) into an NM one (at lower volumes). This prevented us from determining the total energy minimum for the FM state. Therefore, unless explicitly mentioned, in the following we discuss properties of the NM θ-Ni_4N phase only. Further, the local magnetic moments of Ni atoms in the δ-Ni4N phase are so small and so close to our numerical accuracy that we consider this state as effectively non-magnetic. Here the energies of both FM and NM states are nearly identical.

The calculated structural characteristics are summarized in Tables III and IV for each structure in its minimum-energy state. In particular, the equilibrium volume V_{eq} (in Å^3 per atom), the lattice parameter a (in Å) and the b/a and c/a ratios in the case of noncubic phases, as well as relaxed internal parameters of Ni (N) atomic positions $^{\mathrm{Ni}}u$ ($^{\mathrm{N}}u$) are listed. The

TABLE III. *Ab initio* calculated equilibrium values of the atomic volume V_{eq}, lattice parameter a, the ratios between lattice parameters b/a and c/a, and calculated values of the magnetic moment μ per Ni atom of ferromagnetic (FM) states. The δ-Ni_4N phase is effectively non-magnetic (NM).

Ni_4N	V_{eq} (Å^3/atom)	a (Å)	b/a	c/a	μ (μ_B/Ni)
α (FM)	10.40	3.73	1	1	0.396
α expt.[13]	10.72	3.77	1	1	
β (NM)	10.16	5.75	1	1.07	
γ (NM)	10.28	5.02	1.2	1.36	
δ (NM)	10.37	6.07	0.96	0.96	0.038
ε (FM)	10.35	6.44	0.44	0.44	0.247
ζ (NM)	10.82	3.78	1	1	
η (NM)	11.33	4.84	1	1	
θ (NM)	10.14	3.55	1	2.27	

TABLE IV. Ground-state values of internal structural parameters determining atomic positions (see Table XI in the Appendix for details) on different Wyckoff sublattices (these are indicated by superscripts).

Ni_4N	β	γ	ε	ζ	η	θ
$^{\mathrm{N}}u^x$		0.0^{4c}				
$^{\mathrm{N}}u^z$		0.0^{4c}				0.164^{2c}
$^{\mathrm{Ni}}u^x$	0.034	0.197^{4c}	0.219^{2l}	0.268^{4c}	0.287^{8c}	
$^{\mathrm{Ni}}u^z$		0.5^{4c}				0.5^{2c}
$^{\mathrm{Ni}}u^x$		0.5^{8d}				
$^{\mathrm{Ni}}u^y$		0.5^{8d}				
$^{\mathrm{Ni}}u^z$		0.717^{8d}				0.286^{4f}

volumetric dependences of internal parameters $^{\mathrm{Ni}}u$ and $^{\mathrm{N}}u$ defined for the β-Ni_4N, γ-Ni_4N, ε-Ni_4N, ζ-Ni_4N, η-Ni_4N, and θ-Ni_4N structural variants are shown in Figs. 7 and 8.

Inspecting the volumetric dependences in Figs. 7 and 8 we see that the internal parameter $^{\mathrm{Ni}}u$ in the η-Ni_4N structural variant is rather constant for lower volumes, equal to the value 0.25 that corresponds to the Ni atoms being located in exactly one-quarter along the body diagonal of the elementary unit cell (see the upper left part of Fig. 4). This trend changes at about 8.5 Å^3 per atom and the internal parameter $^{\mathrm{Ni}}u$ increases for higher volumes. In order to examine the impact of these changes on the energetics of the η-Ni_4N allotrope (see a similar analysis in the case of $MoSi_2$ in Refs. 55 and 56), we have performed also a series of calculations with $^{\mathrm{Ni}}u = 0.25$ and these data points are marked as η^* in Fig. 6. Apparently, rather small changes in the value of the internal parameter $^{\mathrm{Ni}}u$ result in quite significant reduction of the total energy of the η-Ni_4N compound.

Similarly, a geometrically ideal position with $^{\mathrm{Ni}}u = 0.25$ may occur in the ζ-Ni_4N phase that, in contrast to the trend detected in the η-Ni_4N allotrope, reaches this value only for the highest studied volumes. Also in this case we fixed the internal parameter $^{\mathrm{Ni}}u$ to 0.25 and the corresponding data points are

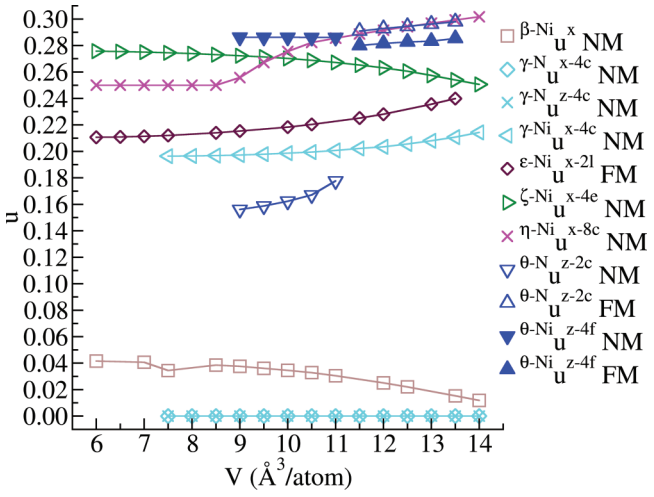

FIG. 7. (Color online) *Ab initio* calculated volumetric dependences of internal atomic-position parameter $^{\mathrm{N}}u$ and $^{\mathrm{Ni}}u$ (see also Table IV) in β-Ni_4N, ε-Ni_4N, ζ-Ni_4N, γ-Ni_4N, η-Ni_4N, and θ-Ni_4N allotropes.

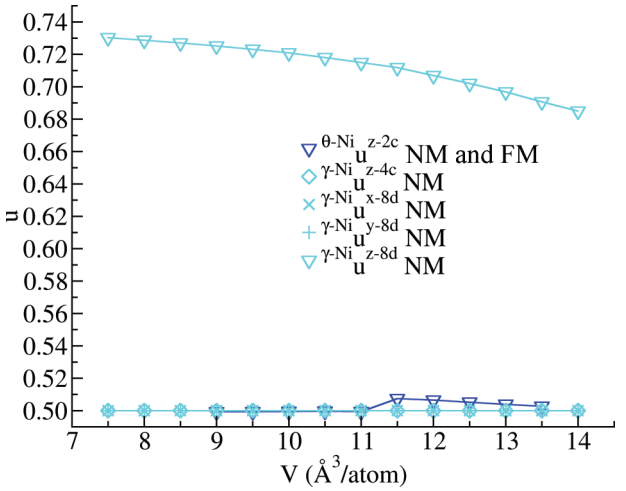

FIG. 8. (Color online) *Ab initio* calculated volumetric dependences of internal atomic-position parameter $^{\mathrm{Ni}}u$ (see also Table IV) in γ-Ni_4N and θ-Ni_4N allotropes.

labeled ζ^* in Fig. 6. Again, a significant reduction of the total energy is seen when compared with the unconstrained states.

Employing the Murnaghan equation of state[40] for the total energy E,

$$E(V) = E_0 + \frac{B_0 V}{B_0'}\left(\frac{(V_0/V)^{B_0'}}{B_0' - 1} + 1\right) - \frac{B_0 V_0}{B_0' - 1},$$

we can express the energy E as a function of the pressure p applying the analysis performed recently by Holec *et al.*,[57]

$$E(p) = E_0 + \frac{B_0 V_0}{B_0' - 1}\left[\frac{\frac{p}{B_0} + 1}{\sqrt[B_0']{\frac{B_0'}{B_0}p + 1}} - 1\right],$$

using the pressure dependence derived from the Murnaghan equation of state:

$$p = -\frac{\partial E}{\partial V} \quad \Rightarrow \quad V(p) = \frac{V_0}{\sqrt[B_0']{\frac{B_0'}{B_0}p + 1}}.$$

The pressure dependences of the atomic volume for all studied phases determined in this way are shown in Fig. 9. Based on this relation, the enthalpy $H(p) = E[V(p)] + pV(p)$ can be evaluated analytically and the corresponding pressure dependences are visualized in Fig. 10. The results indicate that within the considered pressure range the order of thermodynamic stability is not altered with the only exception being the two phases with the highest energies considered in our study, η and θ, for which enthalpies cross at ≈8 GPa.

As far as elastic parameters are concerned, selected computed values are summarized in Table V for each structure. In particular, the bulk modulus B (in GPa) and its pressure derivative B' (as a representative of third-order elastic constants) are listed. It is worth noting that the most stable α-Ni_4N allotrope (see a detailed analysis below) possesses also the highest value of the bulk modulus $B = 197$ GPa. In contrast, the lowest value is predicted for η-Ni_4N.

In order to obtain energy-related quantities characterizing the thermodynamic stability, such as the formation energy of the studied nickel nitrides, the ground-state energies of

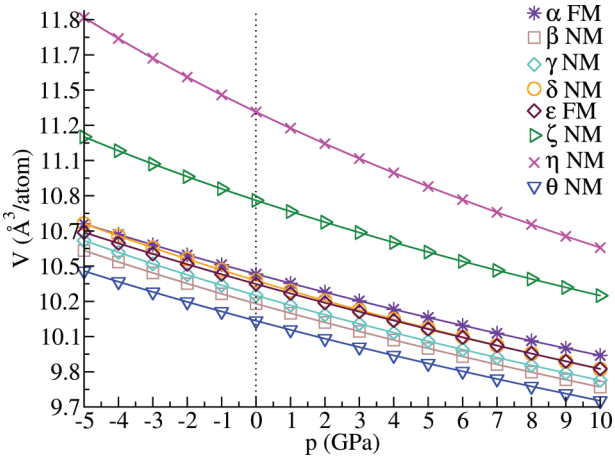

FIG. 9. (Color online) Atomic volume V (in Å^3 per atom) as function of pressure of the various Ni_4N phases.

the elemental constituents must be known. Therefore, we calculated the energy-volume dependence for ferromagnetic (FM) and nonmagnetic (NM) fcc and bcc nickel. To obtain an upper bound for the nitrogen chemical potential, we employ a large cube-shaped supercell (with the lattice parameter $a = 11$ Å) with a two-atomic nitrogen molecule N_2 inside and optimized the N-N interatomic distance so as to minimize the total energy. The calculated lattice parameter of FM fcc Ni (3.52 Å) agrees excellently with the measured value (3.524 Å[58]). Similarly, good agreement is reached between computed (1.117 Å) and measured (1.097 Å) interatomic distance in the N_2 molecule.[59]

Having obtained the energies of the elemental constituents, we determined the thermodynamic characteristics such as (i) the values of total energy differences ΔE_{TOT} with respect to the most stable structure (the α-Ni_4N allotrope) and (ii) energies of formation E_{f} at $T = 0$ K. The formation energy E_{f} of the studied compounds was calculated using the formula

$$E_{\mathrm{f}}(\mathrm{Ni}_m\mathrm{N}_n) = \frac{E(\mathrm{Ni}_m\mathrm{N}_n) - mE^{\mathrm{Ni}} - nE^{\mathrm{N}}}{m + n},$$

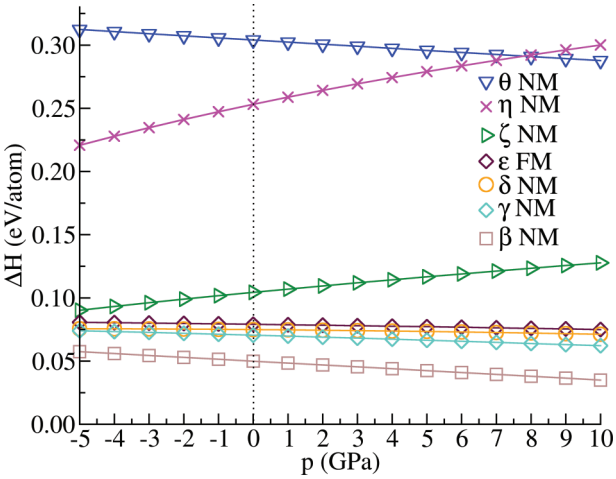

FIG. 10. (Color online) *Ab initio* computed pressure dependence of the enthalpy H for the various Ni_4N phases visualized for each pressure relatively with respect to the enthalpy of the FM α-Ni_4N.

TABLE V. *Ab initio* calculated values of the bulk modulus B (in GPa) and its pressure derivative B' obtained from the Murnaghan equation[40] for V_{eq} (in Å^3 per atom).

Ni_4N	B (GPa)	B'
α (FM)	197	4.9
β (NM)	193	4.4
γ (NM)	182	5.6
δ (NM)	176	5.2
ε (FM)	189	4.2
ζ (NM)	168	5.8
η (NM)	120	4.6
θ (NM)	195	4.9

where $E_f(Ni_mN_n)$ is the total energy (per formula unit) of the Ni_mN_n compound containing m Ni atoms and n N atoms and E^N and E^{Ni} are the total energies per atom of N and Ni in their ground-state phases, i.e., in the N_2 molecule and in ferromagnetic fcc Ni, respectively. These results are listed in Table VI.

Focusing on the $T = 0$ K properties, in particular on the above discussed relation between the thermodynamic stability and the bulk modulus, we can extend our previous discussion about the maximum bulk modulus B found for the most stable compound α-Ni_4N (value of 197 GPa). We therefore combine the bulk modulus values in Table V with the total energy differences ΔE_{TOT} with respect to the α-Ni_4N listed in Table VI; we can also connect the lowest bulk modulus B predicted for the η-Ni_4N phase with the highest value of the total energy differences ΔE_{TOT}, or equivalently with the lowest stability, predicted for the η-Ni_4N compound. In Fig. 11 we draw the dependence of ΔE_{TOT} as a function of the bulk modulus B for all studied compounds. An almost linear relation is observed. The only deviating data point corresponds to the nonmagnetic θ-Ni_4N allotrope. Here we speculate that this compound is so distinctly different from the other studied phases due to its very peculiar cell shape described by a c/a ratio equal to 2.27. Since this phase is also thermodynamically highly unfavorable, we exclude this phase from our subsequent analysis.

Considering the results for the seven remaining compounds, the level of anticorrelation can be mathematically quantified by evaluating the sample correlation coefficient r. For two data sets f_i and g_i, this coefficient is defined as

$$r = \frac{n\sum_{i=1}^{n} f_i g_i - \sum_{i=1}^{n} f_i \sum_{i=1}^{n} g_i}{\sqrt{n\sum_{i=1}^{n} f_i^2 - \left(\sum_{i=1}^{n} f_i\right)^2}\sqrt{n\sum_{i=1}^{n} g_i^2 - \left(\sum_{i=1}^{n} g_i\right)^2}}.$$

If f_i and g_i are strongly anticorrelated, the coefficient approaches -1.

TABLE VI. *Ab initio* calculated values of total-energy differences ΔE_{TOT} with respect to the most stable structure (α-Ni_4N), energy of formation E_f, and for NM phases, the total densities of states (DOS) at the Fermi level.

Ni_4N	ΔE_{TOT} (meV/atom)	E_f (meV/atom)	DOS^{NM} at E_F
α (FM)	0	−48	1.50
β (NM)	53	5	3.50
γ (NM)	70	21	0.96
δ (NM)	77	29	
ε (FM)	84	35	1.12
ζ (NM)	106	57	0.81
η (NM)	255	206	1.47
θ (NM)	306	258	1.55

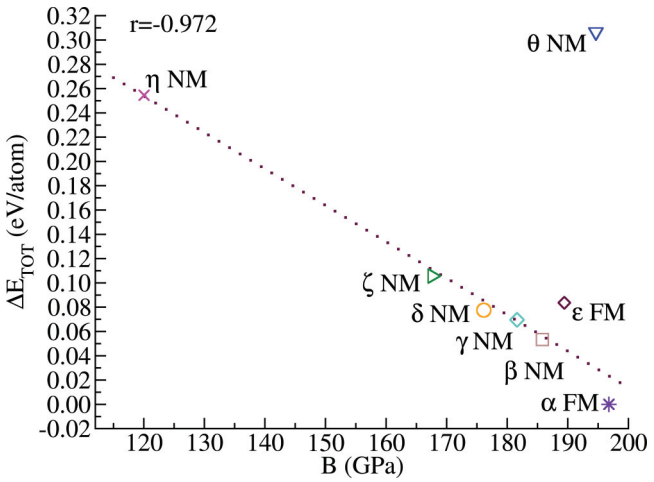

FIG. 11. (Color online) Relation between the total energy difference ΔE_{TOT} with respect to the most stable structure α-Ni_4N and the bulk modulus B (in GPa).

It is seen that the thermodynamical stability (expressed by the total energy difference ΔE_{TOT} with respect to the total energy of the ground-state phase) depends linearly on the bulk modulus B and both quantities are strongly anticorrelated with the sample correlation coefficient r equal to -0.972. The slope of this linear dependence is -3.2 meV/atom per GPa, i.e., an increase of the total energy difference ΔE_{TOT} (or of the formation energy E_f) by 3.2 meV/atom results in a reduction of the bulk modulus B by 1 GPa. This finding is in agreement with recent results related to Ti-Nb bcc alloys[60] or fcc alloys.[61] We note, however, that only the α-Ni_4N compound has negative formation energy E_f indicating that only this phase is thermodynamically stable, whereas all other allotropes are unstable with respect to a decomposition into elemental nickel and nitrogen. This finding is consistent with experimental observations.

After examining selected thermodynamic and elastic properties of the studied Ni_4N allotropes, we further analyze their magnetic characteristics. The calculated values of the atomic magnetic moment μ (per Ni atom) of ferromagnetic (FM) states are listed in Table III. Inspecting the values in Table III we find that only for the ground state α-Ni_4N phase and, to a lesser extent ε-Ni_4N allotrope, a significant magnetic moment occurs. As we can see from Fig. 6, the ground state of θ-phase is probably also FM. Unfortunately, due to convergence problems, we were not able to determine this ground state accurately enough. We can also compare the magnetic moments from Table III with electronic densities of states at the Fermi level ($DOS(E_F)$) computed for NM phases (see Table VI) and consider the Stoner criterion for the occurence of magnetism. Interestingly, we do not find any reasonable correlation between a high NM $DOS(E_F)$ and the onset of magnetism.

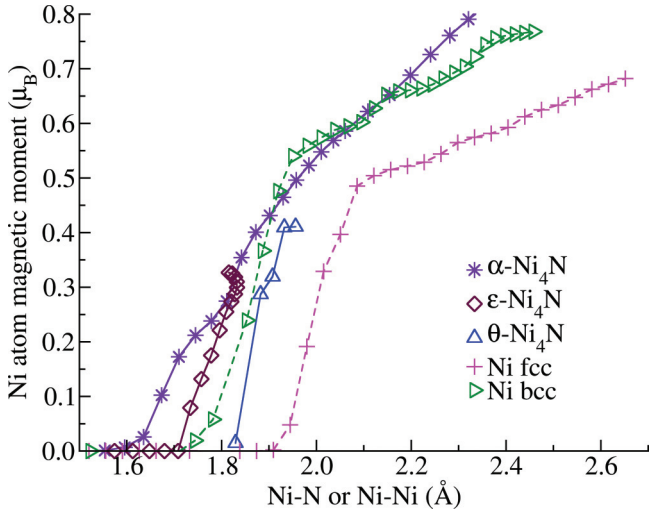

FIG. 12. (Color online) *Ab initio* calculated dependences of magnetic moments μ (per Ni atom) in ferromagnetic (FM) Ni_4N allotropes and fcc and bcc FM Ni as functions of the first-nearest neighbor interatomic distance Ni-N (in case of nickel nitrides) or Ni-Ni (in case of cubic nickel).

In order to compare magnetism in the above mentioned three FM Ni_4N compounds with the FM bcc and fcc Ni phases, we analyze the dependence of the local Ni magnetic moment μ as a function of the distance between the nearest neighboring atoms, i.e., either N-Ni (in Ni_4N compounds) or Ni-Ni (in fcc and bcc FM Ni). The trends are depicted in Fig. 12. It turns out the onset of magnetism in the Ni_4N FM compounds and in elemental Ni is connected with the interatomic distances between 1.6 and 1.9 Å with the lower value found mostly for nickel nitrides and the upper value in the elemental FM fcc Ni. The trends in Fig. 12 are qualitatively quite similar for nickel nitrides and pure Ni, though not identical. Both bcc and fcc Ni exhibit a well-pronounced kink on the dependence of the local magnetic moment on the nearest-neighbor interatomic distance that is shifted to a lower value in the case of hypothetical bcc Ni. In contrast to that, dependences obtained for nickel nitrides exhibit also changes of the slope but these are less pronounced.

Having found common features in the magnetism of Ni_4N compounds and Ni states, we continue our study with a detailed description of single-crystalline elastic properties of the ground-state cubic α-Ni_4N phase. The comparison of these results with single-crystalline elastic constants computed for fcc FM Ni is given in Table VII (results for noncubic tetragonal-symmetry β-Ni_4N are summarized in Table XII in the Appendix for a future reference). For nitrides possessing a cubic symmetry, we calculated all three single-crystalline elastic constants as well as homogenized polycrystalline elastic moduli and compared the results with those obtained for fcc FM Ni (see Table VIII). As seen in Table VII, our theoretically predicted single-crystalline elastic constants of FM fcc Ni agree very well with the measured ones.[58]

TABLE VII. Summary of *ab initio* calculated and experimental second order single-crystal elastic constants C_{11}, C_{12}, C_{44} and the Zener anisotropy ratio $A_Z = 2C_{44}/(C_{11} - C_{12})$ of ferromagnetic (FM) fcc nickel and α-Ni_4N, ζ-Ni_4N, and η-Ni_4N.

	C_{11} (GPa)	C_{12} (GPa)	C_{44} (GPa)	A_Z
Ni this work	268	151	129	2.20
Ni expt.[58]	248	155	124	2.67
α-Ni_4N (FM)	348	121	43	0.38
ζ-Ni_4N (NM)	181	161	114	11.4
η-Ni_4N (NM)	251	55	50	0.51

TABLE VIII. *Ab initio* calculated polycrystalline shear moduli G, Young moduli Y, and Poisson ratios ν of the cubic α-Ni_4N, ζ-Ni_4N, and η-Ni_4N phases. Voigt (V), Reuss (R), Hershey (H), as well as Reuss-Voigt-Hill-Gilvarry (RVHG) homogenization schemes are used. Specifically for the Hershey's homogenization method we also list B/G ratios. For the sake of completeness, Cauchy pressures C_{12}-C_{44} are given, too.

	α-Ni_4N	ζ-Ni_4N	η-Ni_4N	fcc FM Ni
G_V (GPa)	71	72	69	101
Y_V (GPa)	191	190	174	257
ν_V	0.306	0.276	0.223	0.239
G_H (GPa)	64	49	65	94
Y_H (GPa)	173	133	166	243
ν_H	0.322	0.338	0.234	0.251
B/G_H	3.09	3.44	1.84	2.01
C_{12}-C_{44}	78	47	5	22
G_{RVHG} (GPa)	64	47	66	94
Y_{RVHG} (GPa)	174	130	167	242
ν_{RVHG}	0.321	0.342	0.233	0.252
G_R (GPa)	57	22	62	87
Y_R (GPa)	156	63	159	227
ν_R	0.338	0.419	0.244	0.266

The anisotropic single-crystalline elastic response is conveniently visualized by calculating the directional dependence of the Young modulus $Y(\mathbf{r})$ and our results are shown in Fig. 13. Apparently, the α-Ni_4N compound is both quantitatively and qualitatively different from the elemental fcc Ni. The maximum values (indicated by dark blue-red color) are comparable but the crystallographic directions are complementary, i.e., the [001] is the softest and the [111] the hardest direction in the case of α-Ni_4N phase, but it is the other way around in FM fcc Ni. The difference may also be conveniently characterized by Zener's anisotropy A_Z ratio that for the three cubic Ni_4N allotropes reaches rather extreme values. In contrast to FM fcc Ni with the Zener's ratio equal to 2.20, its value is as low as 0.38 and 0.51 for α-Ni_4N and η-Ni_4N, respectively, but as high as 11.4 in case of ζ-Ni_4N. The very low values predicted for α-Ni_4N and η-Ni_4N are clearly due to rather low values of C_{44} (see Table VII) similarly as, e.g., in the case of α-Po crystallizing in the simple cubic structure (for details, see Refs. 62–64). Exactly in opposite manner, the very high value of 11.4 computed for ζ-Ni_4N is due to an extremely low value of $C' = 1/2(C_{11} - C_{12})$.

Additionally, we also list in Table VIII the ratio of the bulk and shear moduli employing Hershey's homogenization method as well as the Cauchy pressures. The former parameter, the B/G ratio, was found to be correlated with the ductility of materials.[65] We find all phases to have the ratio above the threshold of 1.75 separating materials behaving in a brittle

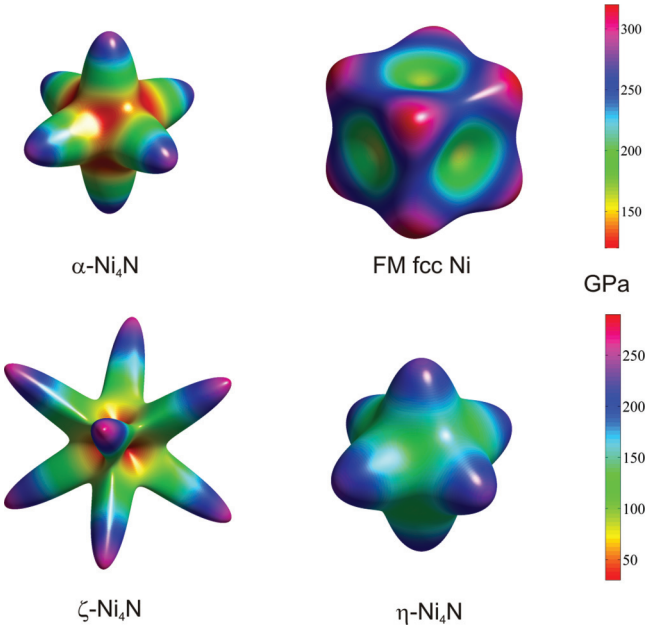

FIG. 13. (Color online) *Ab initio* predicted directional dependence of single-crystalline Young modulus for FM α-, NM ζ-, and NM η-Ni_4N, as well as for ferromagnetic fcc Ni.

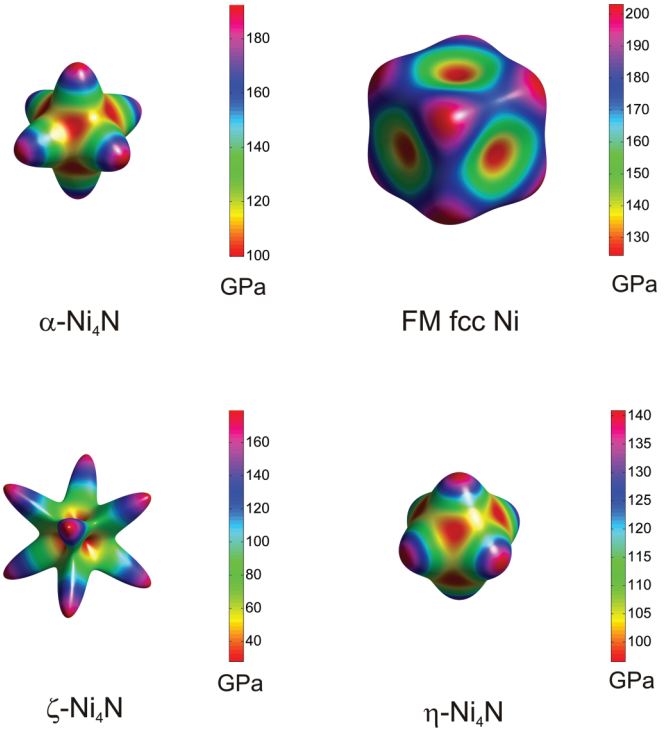

FIG. 14. (Color online) Computed directional dependences of single-crystalline area modulus A of FM α-Ni_4N, fcc FM Ni, NM ζ-Ni_4N, and NM η-Ni_4N.

manner ($B/G < 1.75$) from those that are ductile ($B/G > 1.75$) and we thus expect these compounds to be ductile rather than brittle.

Also the positive Cauchy pressure supports this prediction as negative values are commonly interpreted as a fingerprint of covalent bonds[66] appearing in brittle materials. Recently, however, it was demonstrated that the Cauchy pressure is negative not because of covalent bonding as originally suggested but because of long-range electrostatic potential contributions.[67]

To study the elastic response of Ni_4N cubic phases to biaxial strains, we have also analyzed directional dependence of the area modulus $A(\mathbf{r})$ as recently introduced, e.g., in Refs. 68 and 69. The area modulus is a two-dimensional counterpart of the Young's modulus. In a similar manner as the Young's modulus describes uniaxial loadings along a vector $\mathbf{r}$, the area modulus describes the change of the area within a plane with the plane normal vector $\mathbf{r}$. Specifically, for cubic systems, the area modulus $A(\mathbf{r})$ may be obtained from the relation

$$\frac{1}{A(\mathbf{r})} = \frac{1}{Y(\mathbf{r})} + \frac{1}{3B}. \tag{16}$$

The area modulus is a useful visualization of the amount of elastic energy that is necessary, for example, for epitaxial deposition of a studied material on a substrate in a fully coherent manner. Figure 14 can be thus interpreted that the elastic energy will be lowest when α-Ni_4N is grown to interface a substrate by its {111} planes and highest for {100} planes. Similar conclusions can be drawn for the η-Ni_4N allotrope. For the ζ-Ni_4N phase, due to its qualitatively opposite elastic anisotropy as compared with α-Ni_4N, planes minimizing and maximizing the elastic energy in case of epitaxial growth will be exactly inverted.

Due to the fact that both thin films and grain-boundary precipitates typically exist in rather complex stress/strain states, we also calculated the pressure dependence of single-crystalline elastic constants. As shown in Figs. 15, 16, and 17 C_{11} and C_{44} increase with increasing hydrostatic pressure but C_{12} decreases. The computed trends allow for comparison with those predicted by *ab initio* methods in other nitrogen-containing cubic intermetallics and alloys, such as zinc-blende III-N nitrides,[70,71] cubic boron nitrides,[72–74] superhard semiconducting C_3N_2,[75] cubic spinel $SiGe_2N_4$,[76] cubic antiperovskites (i) $ANSr(3)$ (A = As, Sb, and Bi),[77] (ii) $AsNBa_3$ and $SbNBa_3$,[78] and (iii) $MNNi3$ (M = Zn, Cd, Mg, Al, Ga, In, Sn, Sb, Pd, Cu, Ag, and Pt),[79] cubic TiN and AlN,[80] cubic phases of NbN[81] and GaN,[82] zinc-blende and rocksalt BN,[83] ultraincompressible bimetallic interstitial

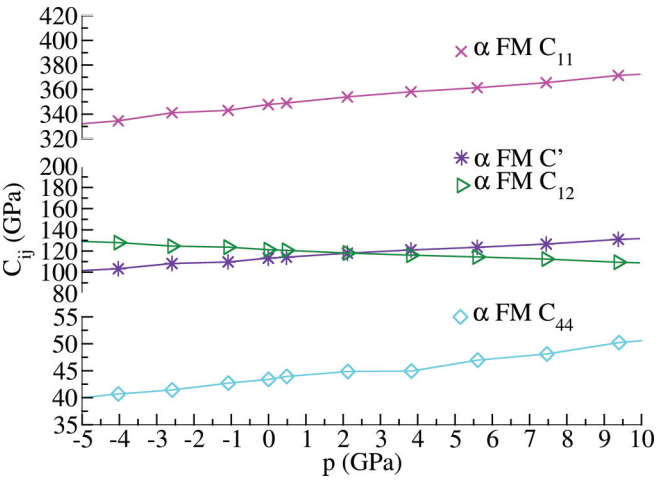

FIG. 15. (Color online) *Ab initio* calculated pressure dependences of single-crystalline elastic constants of the FM α-Ni_4N phase.

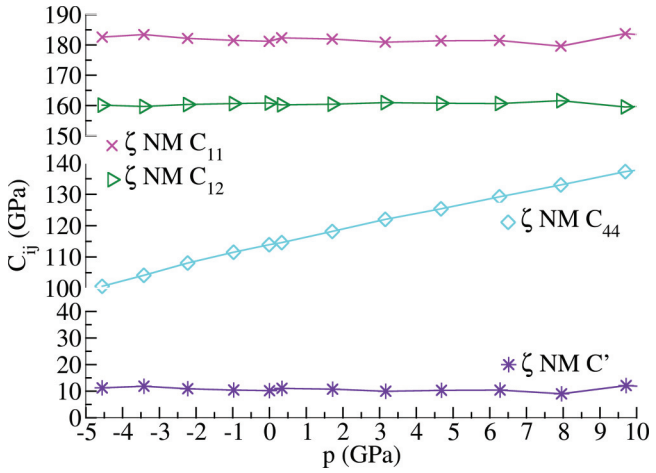

FIG. 16. (Color online) *Ab initio* calculated pressure dependences of single-crystal elastic constants of the NM ζ-Ni_4N phase.

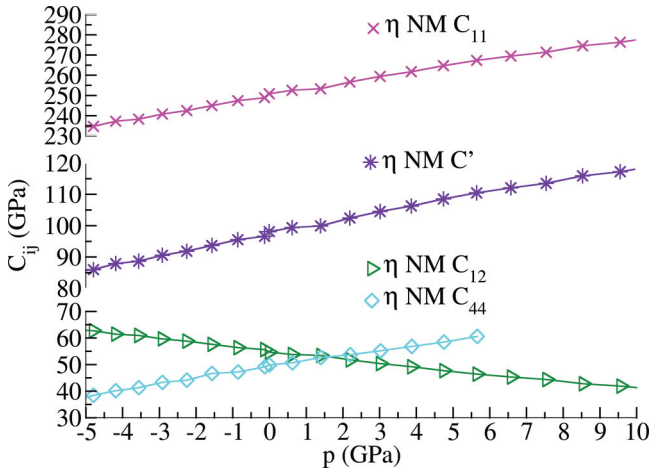

FIG. 17. (Color online) *Ab initio* calculated pressure dependences of single-crystal elastic constants of the NM η-Ni_4N phase.

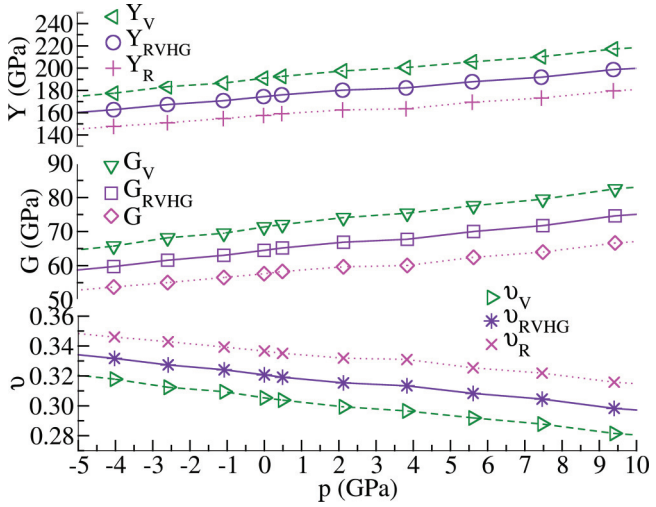

FIG. 18. (Color online) Calculated pressure dependences of homogenized elastic moduli (Young Y and shear G) together with the Poisson ratio ν of the FM α-Ni_4N phase as obtained employing Voigt, Reuss, and Reuss-Voigt-Hill-Gilvarry (RVHG) homogenization schemes. The data points using the Hershey's method are not shown as they are very similar to the RVHG ones.

TABLE IX. Extremal values of Poisson ratio $\nu(\mathbf{n},\mathbf{m})$ for a uniaxial loading along the vector **n** and perpendicular strain in the direction **m**.

	ν_{min}	**n**	**m**	ν_{max}	**n**	**m**
α-Ni_4N	0.127	[1 1 0]	[0 0 1]	0.635	[1 1 0]	[1 $\bar{1}$ 0]
ζ-Ni_4N	−0.625	[1 1 0.388]	[1 $\bar{1}$ 0]	1.43	[1 1 0]	[0 0 1]
η-Ni_4N	0.115	[1 1 0]	[0 0 1]	0.476	[1 1 0]	[1 $\bar{1}$ 0]

nitrides Ni_2Mo_3N, Pd_2Mo_3N, Pt_2Mo_3N, Co_3Mo_3N, and Fe_3Mo_3N,[84] or C_3N_2,[85] Zr_3N_4, and Hf_3N_4.[86]

By applying homogenization techniques, the pressure dependence of polycrystalline Young and shear moduli as well as of the Poisson ratio ν have been obtained for FM α-Ni_4N allotrope and are visualized in Fig. 18. It can be seen that polycrystalline elastic moduli increase with increasing hydrostatic pressure while the Poisson ratio decreases.

We have also tested stability conditions based on these single-crystalline elastic constants at different hydrostatic pressures p (for details see, e.g., Refs. 87–90),

$$C_{11} - C_{12} - p > 0, \tag{17}$$

$$C_{11} + 2C_{12} + 2p > 0, \tag{18}$$

$$C_{44} - p/2 > 0, \tag{19}$$

within the studied pressure range. These stability conditions are the same as, e.g., relations (C.5) from Ref. 89 or the lowest set of relations (48) from Ref. 90. For the α-Ni_4N phase all conditions are obeyed and we can conclude that it is predicted to be mechanically stable.

Finally, our extended analysis of single-crystalline elastic constants for all three cubic variants allows one to examine Poisson ratios for loadings along different directions. Following the analysis by Norris,[69] extremal values have been determined and these are summarized in Table IX. Seeing negative values of Poisson's ratio in the case of ζ-Ni_4N we can conclude that, if this phase could be prepared (e.g., in thin films under external constraints), it would have auxetic properties on the single-crystalline level, i.e., due to an uniaxial tension along the [1 1 0.388] direction, this material would expand in the [1$\bar{1}$0] direction perpendicular to the loading axis.

IV. CONCLUSIONS

With the help of *ab initio* methods, we studied thermodynamic, structural, magnetic, elastic, and electronic properties of eight allotropes of Ni_4N. Our theoretical results confirm, in agreement with experimental findings, that the cubic allotrope [Pearson symbol cP5, space group $Pm\bar{3}m$ (221)] is the most stable one within the studied set. It is also the only one thermodynamically stable at $T = 0$ K with respect to the decomposition to the elemental Ni and the N_2 gas phase. For all eight allotropes, we determined the lattice and internal structural parameters, as well as the bulk moduli and their pressure derivatives. The thermodynamic stability and bulk modulus were found to be anticorrelated.

By analyzing both spin-polarized ferromagnetic and nonmagnetic states we find similarities between the behavior of magnetic moment as a function of Ni-N and Ni-Ni nearest neighbor distance in the elemental Ni and studied ferromagnetic phases of Ni_4N. Aiming mostly at the ground-state Ni_4N

allotrope, a complete set of single-crystalline elastic constants is calculated at both zero and gigapascal hydrostatic pressures. These values are further homogenized in order to predict polycrystalline elastic moduli employing Voigt, Reuss, Hershey, and Reuss-Voigt-Hill-Gilvarry homogenization methods.

Finally, we demonstrate that the elastic anisotropy of the ground-state Ni_4N allotrope is both quantitatively and qualitatively different from that in elemental fcc Ni as they have opposite hard and soft crystallographic directions. Further, for one of the cubic phase we show that it possesses a negative Poisson ratio, indicating an auxetic material on the single-crystalline level. As there is very little experimental information on metastable phases of Ni_4N that can possibly exist at elevated temperatures as well as on their materials properties, most of the present results are theoretical predictions which may motivate future experimental work.

ACKNOWLEDGMENTS

This research was supported by the Grant Agency of the Czech Republic (Projects No. GAP108/12/0311 and No. GD106/09/H035), the Grant Agency of the Academy of Sciences of the Czech Republic (Project No. IAA100100920), the Project CEITEC − Central European Institute of Technology (CZ.1.05/1.1.00/02.0068) from the European Regional Development Fund, and the Academy of Sciences of the Czech Republic (Institutional Project No. RVO:68081723). M.F. would like to acknowledge the funding by the Fellowship of Jan Evangelista Purkyně of the Academy of Sciences of the Czech Republic, and by the Interdisciplinary Centre for Materials Simulation (ICAMS), which is supported by ThyssenKrupp AG, Bayer MaterialScience AG, Salzgitter Mannesmann Forschung GmbH, Robert Bosch GmbH, Benteler Stahl/Rohr GmbH, Bayer Technology Services GmbH, the State of North-Rhine Westphalia, and the European Commission in the framework of the European Regional Development Fund. The access to the MetaCentrum computing facilities provided under the program "Projects of Large Infrastructure for Research, Development, and Innovations"(No. LM2010005), funded by the Ministry of Education of the Czech Republic, is greatly appreciated.

APPENDIX

Tables X, XI, and XII contain optimized atomic positions, crystallographic description of the studied phases, and *ab initio* calculated single-crystalline elastic constants of the β-Ni_4N phase, respectively.

TABLE X. Optimized atomic positions in the δ-Ni_4N Lifshitz structure after full relaxation. Let us note that the relaxed nickel Wyckoff positions are quite different from the "ideal" unrelaxed ones that are given in Table II.

Wyckoff positions Ni
(0.3028, −0.0211, 0.0211); (0.2500, 0.5219, 0.0219)
(0.6972, 0.0211, −0.0211); (0.7500, 0.4781, −0.0219)
(0.0000, 0.2281, 0.2281); (−0.0528, 0.7711, 0.2289)
(0.5000, 0.2719, 0.2719); (0.5528, 0.7289, 0.2711)
(0.2500, −0.0219, 0.4781); (0.1972, 0.5211, 0.4789)
(0.7500, 0.0219, 0.5219); (0.8028, 0.4789, 0.5211)
(0.0528, 0.2289, 0.7711); (0.0000, 0.7719, 0.7719)
(0.4472, 0.2711, 0.7289); (0.5000, 0.7281, 0.7281)

TABLE XI. Crystallographic description of the studied phases (without the Lifshitz structure δ-Ni_4N, which is given in Table II). For the notation of the internal parameter u, see the caption of Table II.

Ni_4N	Wyckoff positions N	Wyckoff positions Ni
α	1a (0, 0, 0)	1b (1/2, 1/2, 1/2)
		3d (1/2, 0, 0)
		(0, 1/2, 0)
		(0, 0, 1/2)
β	(1/4, 1/4, 1/4)	(1/4, 0, 0)
	(3/4, 3/4, 1/4)	(3/4, 0, 0)
	(3/4, 1/4, 3/4)	(1/4, 1/2, 0)
	(1/4, 3/4, 3/4)	(3/4, 1/2, 0)
		(1/4, 0, 1/2)
	$^{Ni}u^x = 0.034$	(1/4, 1/2, 1/2)
		(3/4, 0, 1/2)
		(3/4, 1/2, 1/2)
		$(1 - {}^{Ni}u^x, 1/4, 1/4)$
		$({}^{Ni}u^x, 3/4, 1/4)$
		$(1/2 + {}^{Ni}u^x, 1/4, 1/4)$
		$(1/2 - {}^{Ni}u^x, 3/4, 1/4)$
		$({}^{Ni}u^x, 1/4, 3/4)$
		$(1 - {}^{Ni}u^x, 3/4, 3/4)$
		$(1/2 - {}^{Ni}u^x, 1/4, 3/4)$
		$(1/2 + {}^{Ni}u^x, 3/4, 3/4)$
γ	4c $(u^x, 1/4, u^z)$	4c $(u^x, 1/4, u^z)$
	$(1/2 - u^x, 3/4, 1/2 + u^z)$	$(1/2 - u^x, 3/4, 1/2 + u^z)$
	$(1 - u^x, 3/4, 1 - u^z)$	$(1 - u^x, 3/4, 1 - u^z)$
	$(1/2 + u^x, 1/4, 1/2 - u^z)$	$(1/2 + u^x, 1/4, 1/2 - u^z)$
		4c $(u^x, 1/4, u^z)$
	$^{N}u^{x-4c} = 0.0$	$(1/2 - u^x, 3/4, 1/2 + u^z)$
	$^{N}u^{z-4c} = 0.0$	$(1 - u^x, 3/4, 1 - u^z)$
	$^{Ni}u^{x-4c} = 0.197$	$(1/2 + u^x, 1/4, 1/2 - u^z)$
	$^{Ni}u^{z-4c} = 0.5$	8d (u^x, u^y, u^z)
	$^{Ni}u^{x-8d} = 0.5$	$(1 - u^x, 1 - u^y, 1 - u^z)$
	$^{Ni}u^{y-8d} = 0.5$	$(1/2 - u^x, 1 - u^y, 1/2 + u^z)$
	$^{Ni}u^{z-8d} = 0.717$	$(1/2 + u^x, u^y, 1/2 - u^z)$
		$(1 - u^x, 1/2 + u^y, 1 - u^z)$
		$(u^x, 1/2 - u^y, u^z)$
		$(1/2 + u^x, 1/2 - u^y, 1/2 - u^z)$
		$(1/2 - u^x, 1/2 + u^y, 1/2 + u^z)$
ε	1h (1/2, 1/2, 1/2)	1a (0, 0, 0)
		1b (1/2, 0, 0)
	$^{Ni}u^{x-2l} = 0.219$	2l $(u^x, 1/2, 1/2)$
		$(1 - u^x, 1/2, 1/2)$
ζ	1a (0, 0, 0)	4e (u^x, u^x, u^x)
		$(1 - u^x, 1 - u^x, u^x)$
	$^{Ni}u^{x-4c} = 0.268$	$(1 - u^x, u^x, 1 - u^x)$
		$(u^x, 1 - u^x, 1 - u^x)$
η	2a (0, 0, 0)	8c (u^x, u^x, u^x)
	(1/2, 1/2, 1/2)	$(1 - u^x, 1 - u^x, u^x)$
		$(1 - u^x, u^x, 1 - u^x)$
	$^{Ni}u^{x-8c} = 0.287$	$(u^x, 1 - u^x, 1 - u^x)$
		$(1/2 + u^x, 1/2 + u^x, 1/2 + u^x)$
		$(1/2 - u^x, 1/2 - u^x, 1/2 + u^x)$
		$(1/2 - u^x, 1/2 + u^x, 1/2 - u^x)$
		$(1/2 + u^x, 1/2 - u^x, 1/2 - u^x)$
θ	2c (0, 1/2, z)	2a (0, 0, 0)
	$(1/2, 0, 1 - u^z)$	(1/2, 1/2, 0)
		2c $(0, 1/2, u^z)$
	$^{N}u^{z-2c} = 0.164$	$(1/2, 0, 1 - u^z)$
	$^{Ni}u^{z-2c} = 0.5$	4f $(0, 0, u^z)$
	$^{Ni}u^{z-4f} = 0.286$	$(1/2, 1/2, u^z)$
		$(1/2, 1/2, 1 - u^z)$
		$(0, 0, 1 - u^z)$

TABLE XII. *Ab initio* calculated single-crystalline elastic constants of β-Ni_4N (following the computational approach published in Ref. 91).

	C_{11} (GPa)	C_{12} (GPa)	C_{13} (GPa)	C_{33} (GPa)	C_{44} (GPa)	C_{66} (GPa)
C_{ij} β-Ni_4N	230	153	156	235	64	40

*mafri@ipm.cz

[1] J. Guo, F. Pan, M. Feng, R. Guo, P. Chou, and C. Chang, J. Appl. Phys. **80**, 1623 (1996).

[2] J. Kim, J. Je, J. Lee, Y. Park, and B. Lee, J. Electrochem. Soc. **147**, 4645 (2000).

[3] J. Kim, J. Je, J. Lee, Y. Park, T. Kim, I. Jung, B. Lee, and J. Lee, J. Electron. Mater. **30**, L8 (2001).

[4] C. Kim, J. Kim, J. Lee, J. Je, M. Yi, D. Noh, Y. Hwu, and P. Ruterana, in *4th International Conference on Nitride Semiconductors (ICNS-4), Denver, Colorado, 2001* [Phys. Status Solidi A **188**, 379 (2001)].

[5] R. Valencia, R. Lopez-Callejas, A. Munoz-Castro, S. Barocio, E. Chavez, and O. Godoy-Cabrera, in *10th Latin American Workshop on Plasma Physics/7th Brazilian Meeting on Plasma Physics, Sao Pedro, Brazil, 2003* [Braz. J. Phys. **34**, 1594 (2004)].

[6] H. Savaloni and M. Habibi, Appl. Surf. Sci. **258**, 103 (2011).

[7] E. Menthe, A. Bulak, J. Olfe, A. Zimmermann, and K. T. Rie, Surf. Coat. Technol. **133**, 259 (2000).

[8] L. Zagonel, C. Figueroa, R. Droppa, Jr., and F. Alvarez, Surf. Coat. Technol. **201**, 452 (2006).

[9] B. Larisch, U. Brusky, and H. J. Spies, Surf. Coat. Technol. **116**, 205 (1999).

[10] L. Zagonel, C. Figueroa, and F. Alvarez, Surf. Coat. Technol. **200**, 2566 (2005).

[11] A. Leineweber, H. Jacobs, and S. Hull, Inorg. Chem. **40**, 5818 (2001).

[12] C. Q. Sun, Vacuum **52**, 347 (1999).

[13] I. M. Neklyudov and A. N. Morozov, Physica B **350**, 325 (2004).

[14] S. Desmoulins-Krawiec, C. Aymonier, A. Loppinet-Serani, F. Weill, S. Gorsse, J. Etourneau, and F. Cansell, J. Mater. Chem. **14**, 228 (2004).

[15] Z. Li, R. G. Gordon, V. Pallem, H. Li, and D. V. Shenai, Chem. Mater. **22**, 3060 (2010).

[16] D. L. Kuznetsov, G. G. Ugodnikov, and I. E. Filatov, Tech. Phys. Lett. **34**, 87 (2008).

[17] H. R. Stock, M. Diesselberg, and H. W. Zoch, Surf. Coat. Technol. **203**, 717 (2008).

[18] D. Vempaire, S. Miraglia, A. Sulpice, L. Ortega, E. K. Hlil, D. Fruchart, and J. Pelletier, J. Magn. Magn. Mater. **272-276**, e843 (2004).

[19] Y. Takahashi, Y. Imai, and T. Kumagai, J. Magn. Magn. Mater. **323**, 2941 (2011).

[20] E. Gregoryanz, C. Sanloup, M. Somayazulu, J. Badro, G. Fiquet, H.-K. Mao, and R. J. Hemley, Nat. Mater. **3**, 294 (2004).

[21] A. F. Guillermet and K. Frisk, Int. J. Thermophys. **12**, 417 (1991).

[22] H. A. Wriedt, Bull. Alloy Phase Diagrams **6**, 558 (1985).

[23] C. Guillaume, J. P. Morniroli, D. J. Frost, and G. Serghiou, J. Phys.: Condens. Matter **18**, 8651 (2006).

[24] N. Terao, Naturwissenschaften **46**, 204 (1959).

[25] S. Nagakura, N. Otsuka, and Y. Hirotsu, J. Phys. Soc. Jpn. **35**, 1492 (1973).

[26] S. Nagakura, N. Otsuka, and Y. Hirotsu, Acta Crystallogr. Sect. A **28**, S100 (1972).

[27] P. N. Terao, J. Phys. Soc. Jpn. **15**, 227 (1960).

[28] Y. Kong, J. Pelzl, and F. Li, J. Magn. Magn. Mater. **195**, 483 (1999).

[29] P. Elstnerová, M. Friák, M. Šob, and J. Neugebauer, in *Multi-scale Design of Advanced Materials*, edited by I. Dlouhý, J. Švejcar, and M. Šob (Institute of Physics of Materials, Czech Academy of Sciences, Brno, 2011), p. 27 (in Czech).

[30] P. Hohenberg and W. Kohn, Phys. Rev. **136**, B864 (1964).

[31] W. Kohn and L. J. Sham, Phys. Rev. **140**, A1133 (1965).

[32] J. P. Perdew, K. Burke, and M. Ernzerhof, Phys. Rev. Lett. **77**, 3865 (1996).

[33] G. Kresse and J. Hafner, Phys. Rev. B **47**, 558 (1993).

[34] G. Kresse and J. Furthmüller, Phys. Rev. B **54**, 11169 (1996).

[35] P. E. Blöchl, Phys. Rev. B **50**, 17953 (1994).

[36] H. J. Monkhorst and J. D. Pack, Phys. Rev. B **13**, 5188 (1976).

[37] M. Methfessel and A. T. Paxton, Phys. Rev. B **40**, 3616 (1989).

[38] J. Z. Liu, A. van de Walle, G. Ghosh, and M. Asta, Phys. Rev. B **72**, 144109 (2005).

[39] K. Chen, L. R. Zhao, and J. S. Tse, J. Appl. Phys. **93**, 2414 (2003).

[40] F. D. Murnaghan, Proc. Natl. Acad. Sci. USA **30**, 244 (1944).

[41] A. G. Khachaturyan, *Theory of Structural Transformations in Solids* (John Wiley and Sons, New York, 1983).

[42] A. G. Khachaturyan, Prog. Mater. Sci. **22**, 1 (1978).

[43] A. G. Khachaturyan, Prog. Mater. Sci. **29**, 1 (1985).

[44] W. Voigt, *Lehrbuch der Kristallphysik* (Teubner, Stuttgart, 1928).

[45] A. Reuss, Z. Angew. Math. Mech. **9**, 49 (1929).

[46] A. V. Hershey, J. Appl. Mech. **9**, 49 (1954).

[47] G. Ghosh, S. Delsante, G. Borzone, M. Asta, and R. Ferro, Acta Mater. **54**, 4977 (2006).

[48] G. Ghosh, S. Vaynman, M. Asta, and M. E. Fine, Intermetallics **15**, 44 (2007).

[49] V. A. Lubarda, J. Mech. Phys. Solids **45**, 471 (1997).

[50] D. Holec, M. Friák, J. Neugebauer, and P. H. Mayrhofer, Phys. Rev. B **85**, 064101 (2012).

[51] B.-Y. Tang, N. Wang, W.-Y. Yu, X.-Q. Zeng, and W.-J. Ding, Acta Mater. **56**, 3353 (2008).

[52] H. M. Ledbetter, J. Appl. Phys. **44**, 1451 (1973).

[53] R. Hill, Proc. Phys. Soc. London **65**, 350 (1952).

[54] J. J. Gilvarry, Phys. Rev. **103**, 1701 (1956).

[55] M. Šob and M. Friák, Intermetallics **17**, 523 (2009).

[56] M. Friák, M. Šob, and V. Vitek, Phys. Rev. B **68**, 184101 (2003).

[57] D. Holec, F. Rovere, P. H. Mayrhofer, and P. B. Barna, Scr. Mater. **62**, 349 (2010).

[58] *CRC Handbook of Chemistry and Physics*, 86th ed., edited by D. R. Lide (CRC Press, Boca Raton, FL, 2005).

[59] K. Benran, *Data Handbook for Chemistry*, 3rd ed. (Maruzen Company, Ltd., Tokyo, 1984), Vol. II, pp. 649–661.

[60] L.-F. Zhu, M. Friák, A. Dick, B. Grabowski, T. Hickel, F. Liot, D. Holec, A. Schlieter, U. Kühn, J. Eckert *et al.*, Acta Mater. **60**, 1594 (2012).

[61]S. B. Maisel, M. Höfler, and S. Müller, Nature (London) **491**, 740 (2012).
[62]D. Legut, M. Friák, and M. Šob, Phys. Rev. Lett. **99**, 016402 (2007).
[63]D. Legut, M. Friák, and M. Šob, Phys. Today **61**, 10 (2008).
[64]D. Legut, M. Friák, and M. Šob, Phys. Rev. B **81**, 214118 (2010).
[65]S. F. Pugh, Philos. Mag. Ser. 7 **45**, 823 (1954).
[66]D. G. Pettifor, Mater. Sci. Technol. **8**, 345 (1992).
[67]D. Nguyen-Manh, V. Vitek, and A. P. Horsfield, Prog. Mater. Sci. **52**, 255 (2007).
[68]H. H. Scott, J. Elast. **58**, 269 (2000).
[69]A. N. Norris, Proc. R. Soc. A **462**, 3385 (2006).
[70]S. Lepkowski and J. Majewski, in *33rd International School on Physics of Semiconducting Compounds, Jaszowiec, Poland, 2004* [Acta Phys. Pol. A **105**, 559 (2004)].
[71]S. Lepkowski and J. Majewski, in *GaN, AIN, InN and Their Alloys*, edited by C. Wetzel, B. Gil, M. Kuzuhara, and M. Manfra, MRS Symposia Proceedings No. 831 (Materials Research Society, Pittsburgh, 2005), pp. 647–652.
[72]Y.-D. Guo, X.-S. Song, X.-B. Li, and X.-D. Yang, Solid State Commun. **141**, 577 (2007).
[73]Y. D. Guo, X. D. Yang, X. B. Li, X. S. Song, and X. L. Cheng, Diamond Relat. Mater. **17**, 1 (2008).
[74]J. E. Lowther, Materials **4**, 1104 (2011).
[75]F. Tian, J. Wang, Z. He, Y. Ma, L. Wang, T. Cui, C. Chen, B. Liu, and G. Zou, Phys. Rev. B **78**, 235431 (2008).
[76]M. Moakafi, R. Khenata, A. Bouhemadou, N. Benkhettou, D. Rached, and A. H. Reshak, Phys. Lett. A **373**, 2393 (2009).
[77]M. Hichour, R. Khenata, D. Rached, M. Hachemaoui, A. Bouhemadou, A. H. Reshak, and F. Semari, Phys. B (Amsterdam, Neth.) **405**, 1894 (2010).
[78]P. K. Jha and S. K. Gupta, Solid State Commun. **150**, 1650 (2010).
[79]V. V. Bannikov, I. R. Shein, and A. L. Ivanovskii, Phys. B (Amsterdam, Neth.) **405**, 4615 (2010).
[80]A. J. Wang, S. L. Shang, Y. Du, Y. Kong, L. J. Zhang, L. Chen, D. D. Zhao, and Z. K. Liu, Comput. Mater. Sci. **48**, 705 (2010).
[81]X. Li and J. Du, in *Advances in Civil Engineering, PTS 1-4*, edited by X. Zhou, Applied Mechanics and Materials Vols. 90–93 (Shandong Jianzhu Univ, Sch Civil Engn; Shandong Univ, Sch Civil Engn; Shandong Univ Sci & Technol, Sch Civil Engn & Architecture; Yantai Univ, Sch Civil Engn; Shandong Provincial Key Lab Appraisal & Retrofitt Bldg Struct, Zurich, 2011), pp. 1264–1271.
[82]Z. Usman, C. Cao, G. Nabi, D. Y. Kun, W. S. Khan, T. Mehmood, and S. Hussain, J. Phys. Chem. A **115**, 6622 (2011).
[83]S. Cui, W. Feng, H. Hu, and Z. Feng, Cent. Eur. J. Phys. **8**, 628 (2010).
[84]D. Errandonea, Ch. Ferrer-Roca, D. Martinez-Garcia, A. Segura, O. Gomis, A. Muñoz, P. Rodriguez-Hernández, J. López-Solano, S. Alconchel, and F. Sapiña, Phys. Rev. B **82**, 174105 (2010).
[85]C. Hu, F. Wang, and Z. Zheng, Phys. B (Amsterdam, Neth.) **407**, 3398 (2012).
[86]T. Chihi, M. Fatmi, B. Ghebouli, and M. Guemmaz, Solid State Sci. **13**, 1414 (2011).
[87]J. Wang, J. Li, S. Yip, S. Phillpot, and D. Wolf, Phys. Rev. B **52**, 12627 (1995).
[88]J. W. Morris and C. R. Krenn, Philos. Mag. A **80**, 2827 (2000).
[89]J. Pokluda, M. Černý, J. Šandera, and M. Šob, J. Comput.-Aided Mol. Des. **11**, 1 (2004).
[90]R. Hill and F. Milstein, Phys. Rev. B **15**, 3087 (1977).
[91]J. Y. Suh, Y. S. Lee, J. H. Shim, and H. M. Park, Comput. Mater. Sci. **51**, 365 (2012).